state. In order to get an assignment $J=5/2$, odd parity, for this state using the Austern-Butler-McManus theory, it is necessary that $l=0$ or 4. $l=0$ is ruled out because the angular distribution is clearly not peaked forward, while the first lobe of $j_4(ka)$ with a reasonable choice of nuclear radius, occurs at much too large an angle.

If the restriction $J_y=5/2$ is removed, then one can make a parity and angular momentum assignment consistent with that of Ribe and Seagrave by choosing $l=2$. This yields $J_y=\frac{1}{2}$, $\frac{3}{2}$, 7/2, 9/2 *odd parity*.

It is clear that $j_2(ka)$ will not fit the data as well as $j_1(ka)$; however, it is not certain that the present status of the theory allows one to make a clear distinction.

ACKNOWLEDGMENTS

The authors are indebted to Professor L. W. Alvarez for his interest and encouragement; to Dr. Warren Heckrotte for many instructive discussions on the subject of angular distributions of scattered particles; to William Gantz and Thomas Stand of Hugh Fransworth's Electronics Group for their expert maintenance of the electronic equipment; to Manuel Alcalde and Earl Hosteller for fabrication of the counter components; to William G. Richards for his suggestions and help in constructing the remainder of the equipment made for this experiment; and to all members of the linear accelerator crew, whose cooperation was indispensable to the successful completion of this experiment.

PHYSICAL REVIEW VOLUME 101, NUMBER 2 JANUARY 15, 1956

Quantum Calculation of Coulomb Excitation. II. Quadrupole Excitation: Numerical Results*

L. C. BIEDENHARN,† M. GOLDSTEIN, J. L. MCHALE, AND R. M. THALER
University of California, Los Alamos Scientific Laboratory, Los Alamos, New Mexico

(Received September 26, 1955)

The formal methods for the quantum-mechanical treatment of Coulomb excitation discussed earlier are here applied to obtain numerical results for the electric quadrupole case. Tables of the excitation function and the directional correlation parameters are presented and discussed for a wide range of their arguments.

INTRODUCTION

THE electric quadrupole ($E2$) transition is usually the most strongly favored transition in the Coulomb excitation process[1] and at present one of the most interesting from an experimental point of view. Analysis of the experimental data[2] calls for an accurate treatment of the quadrupole excitation, for both the total cross section and the directional correlation parameters. The semiclassical approximation[3] does not lead to sufficiently accurate results over the entire experimental region.[4] In this paper numerical results for the quantum-mechanical treatment of the electric quadrupole excitation are presented. These results are obtained through the application of the formalism and mathematical techniques for the general multipole in Coulomb excitation, discussed earlier by Biedenharn, McHale, and Thaler.[5] Subsequent work will treat other pure multipoles as well as the cases of mixed transitions.

Results are given for the excitation function and the correlation parameters a_2 and a_4 for values of the arguments in the range $0.1\leqslant\eta\leqslant 15$, $1\leqslant\rho\leqslant 1.4$, where $\eta\equiv Z_1Z_2e^2/\hbar v_{\text{initial}}$ and $\rho\equiv k_{\text{initial}}/k_{\text{final}}$. This range covers energy losses of up to 50% for all energies of experimental interest. Numerical values for computing the total cross section may be taken from Table I. Values for the particle parameters a_2 and a_4 are presented in Tables II and III. These values are plotted in various ways in order to exhibit the general behavior in any region of interest. Such plots should prove helpful in suggesting interpolation procedures.

The limitations of the present treatment have been discussed in I. Of these, the neglect of center of mass corrections is probably the most serious. The results presented below are accordingly most accurate for medium and heavy target nuclei. Neglect of retardation is better justified for quadrupole than other multipole

* Work performed under the auspices of the U. S. Atomic Energy Commission.

† Permanent address: The Rice Institute, Houston, Texas.

[1] A. Bohr and B. Mottelson, Kgl. Danske Videnskab. Selskab, Mat.-fys. Medd. **27**, No. 16 (1953).

[2] P. H. Stelson and F. K. McGowan, Phys. Rev. **98**, 249(A) (1955); F. K. McGowan and P. H. Stelson, Phys. Rev. **99**, 112 (1955).

[3] L. Landau, Physik Z. U.S.S.R. **1**, 88 (1932).

[4] The relevant references to the literature are given in reference 5. The following references should be added to the bibliography given there: K. Mayr [Math. Z. **39**, 597 (1935)]—integrals of Laguerre polynomials in terms of F_2; A. Erdelyi [Math. Z. **40**, 693 (1936)]—confluent hypergeometric integrals evaluated in terms of F_2; J. C. Jaeger [J. London Math. Soc. **13**, 254 (1938)]—an analytic continuation of F_2. In addition, see the following recent papers: Benedict, Daitch, and Breit, Phys. Rev. **101**, 171 (1956); F. D. Benedict, Phys. Rev. **101**, 178 (1956); Breit, Ebel, and Benedict, Phys. Rev. **100**, 428 (1956); Gluckstern, Lazarus, and Breit, Phys. Rev. **101**, 175 (1956).

[5] Biedenharn, McHale, and Thaler, Phys. Rev. **100**, 375 (1955). This paper is referred to as I in the text.

TABLE I. The excitation coefficient a_0 *vs* ρ, η. The coefficient a_0 is tabulated for representative values of its arguments. The entries are presented as four-digit numbers followed by the powers of ten which multiply them.

η \ ρ	1.01	1.02	1.03	1.04	1.05	1.075	1.1	1.2	1.3	1.4
	a_0									
0.1	9.675 −2	9.866 −2	1.005 −1	1.025 −1	1.043 −1	1.092 −1	1.142 −1	1.350 −1	1.566 −1	1.787 −1
0.5	5.170 −2	5.256 −2	5.343 −2	5.430 −2	5.514 −2	5.723 −2	5.919 −2	6.524 −2	6.807 −2	6.797 −2
1.0	2.487 −2	2.520 −2	2.552 −2	2.581 −2	2.605 −2	2.652 −2	2.671 −2	2.509 −2	2.105 −2	1.637 −2
1.5	1.342 −2	1.356 −2	1.368 −2	1.376 −2	1.377 −2	1.365 −2	1.326 −2	1.014 −2	6.578 −3	3.866 −3
2.0	8.125 −3	8.194 −3	8.227 −3	8.210 −3	8.134 −3	7.795 −3	7.240 −3	4.374 −3	2.151 −3	9.425 −4
3.0	3.806 −3	3.811 −3	3.773 −3	3.686 −3	3.555 −3	3.122 −3	2.603 −3	9.278 −4	2.538 −4	6.068 −5
5.0	1.401 −3	1.368 −3	1.281 −3	1.183 −3	1.058 −3	7.387 −4	4.755 −4	5.318 −5	4.288 −6	2.967 −7
8.0	5.422 −4	4.955 −4	4.202 −4	3.379 −4	2.607 −4	1.215 −4	5.066 −5	9.111 −7	1.135 −8	1.201 −10
10.0	3.425 −4	2.935 −4	2.282 −4	1.659 −4	1.148 −4	4.006 −5	1.236 −5	6.440 −8	2.293 −10	6.91_5 −13
15.0	1.422 −4	1.006 −4	6.096 −5	3.362 −5	1.744 −5	2.868 −6	4.100 −7	9.421 −11	1.45_5 −14	···

TABLE II. The particle parameter a_2 *vs* ρ, η. The parameter a_2 is tabulated for representative values of its arguments. The entries are presented as four-digit numbers followed by the powers of ten which multiply them.

η \ ρ	1.01	1.02	1.03	1.04	1.05	1.075	1.1	1.2	1.3	1.4
	a_2									
0.1	4.435 −1	4.624 −1	4.825 −1	5.029 −1	5.238 −1	5.757 −1	6.271 −1	8.183 −1	9.800 −1	1.114 0
0.5	2.279 −1	2.596 −1	2.927 −1	3.265 −1	3.608 −1	4.453 −1	5.265 −1	8.002 −1	9.983 −1	1.142 0
1.0	1.030 −1	1.461 −1	1.920 −1	2.388 −1	2.857 −1	3.980 −1	5.006 −1	8.090 −1	1.002 0	1.130 0
1.5	5.309 −2	1.074 −1	1.654 −1	2.241 −1	2.815 −1	4.142 −1	5.290 −1	8.431 −1	1.021 0	1.132 0
2.0	3.428 −2	1.007 −1	1.712 −1	2.408 −1	3.073 −1	4.550 −1	5.766 −1	8.844 −1	1.046 0	1.144 0
3.0	3.074 −2	1.232 −1	2.170 −1	3.047 −1	3.843 −1	5.487 −1	6.730 −1	9.561 −1	1.092 0	1.171 0
5.0	6.164 −2	2.037 −1	3.330 −1	4.402 −1	5.306 −1	6.987 −1	8.132 −1	1.046 0	1.148 0	1.207 0
8.0	1.283 −1	3.267 −1	4.800 −1	5.956 −1	6.854 −1	8.377 −1	9.336 −1	1.116 0	1.192 0	1.235 0
10.0	1.731 −1	3.985 −1	5.574 −1	6.715 −1	7.575 −1	8.976 −1	9.835 −1	1.143 0	1.209 0	1.24_5 0
15.0	2.783 −1	5.423 −1	6.984 −1	8.036 −1	8.765 −1	9.933 −1	1.062 0	1.184 0	1.23_5 0	···

TABLE III. The particle parameter a_4 *vs* ρ, η. The parameter a_4 is tabulated for representative values of its arguments. The entries are presented as four-digit numbers followed by the powers of ten which multiply them.

η \ ρ	1.01	1.02	1.03	1.04	1.05	1.075	1.1	1.2	1.3	1.4
	a_4									
0.1	5.877 −2	6.569 −2	7.258 −2	7.911 −2	8.514 −2	9.724 −2	1.047 −1	9.117 −2	2.812 −2	−5.983 −2
0.5	2.142 −2	2.695 −2	3.205 −2	3.641 −2	3.988 −2	4.421 −2	4.256 −2	−7.227 −3	−9.002 −2	−1.786 −1
1.0	7.405 −3	1.354 −2	1.886 −2	2.293 −2	2.561 −2	2.650 −2	2.046 −2	−3.961 −2	−1.141 −1	−1.825 −1
1.5	7.245 −3	1.476 −2	2.074 −2	2.470 −2	2.668 −2	2.423 −2	1.422 −2	−5.372 −2	−1.234 −1	−1.816 −1
2.0	8.473 −3	1.716 −2	2.328 −2	2.653 −2	2.722 −2	2.043 −2	6.204 −3	−6.899 −2	−1.360 −1	−1.884 −1
3.0	1.102 −2	2.105 −2	2.603 −2	2.655 −2	2.374 −2	7.951 −3	−1.332 −2	−9.729 −2	−1.596 −1	−2.046 −1
5.0	1.601 −2	2.515 −2	2.462 −2	1.795 −2	8.222 −3	−2.090 −2	−4.985 −2	−1.373 −1	−1.913 −1	−2.273 −1
8.0	2.159 −2	2.371 −2	1.287 −2	−2.638 −3	−1.923 −2	−5.802 −2	−9.031 −2	−1.727 −1	−2.177 −1	−2.462 −1
10.0	2.339 −2	1.956 −2	2.731 −3	−1.692 −2	−3.614 −2	−7.768 −2	−1.101 −1	−1.881 −1	−2.288 −1	-2.54_0 −1
15.0	2.293 −2	4.382 −3	−2.330 −2	−4.870 −2	−7.110 −2	−1.141 −1	−1.449 −1	−2.130 −1	-2.46_0 −1	···

excitations, since the retardation corrections enter to one higher order in $(k_{\text{rad}}r_{tp})^2$.

SUMMARY OF FORMULAS

The electric quadrupole excitation function in the long-wavelength approximation is given by the following expression:

$$b_0=\sum_{l=0}^{\infty}\left[\frac{l(l+1)(2l+1)}{(2l-1)(2l+3)}I^2(l,l)+\frac{3(l+2)(l+1)}{2(2l+3)}\times I^2(l+2,l)+\frac{3l(l-1)}{2(2l-1)}I^2(l-2,l)\right], \quad (1)$$

where

$$I(l,l+m)=\int_0^{\infty}drr^{-3}F_l(\eta_1,k_1r)F_{l+m}(\eta_2,k_2r). \quad (2)$$

In this approximation the total cross section is

$$\sigma_2^{(e)}=4\pi\left(\frac{k_2}{k_1}\right)\left(\frac{2J_f+1}{2J_i+1}\right)(f\|r^2\|i)^2\left(\frac{8\pi Z_1Z_2Me^2}{5k_1k_2\hbar^2}\right)^2 b_0. \quad (3)$$

The reduced radial matrix element in the long-wavelength approximation is

$$Ze(f\|r^2\|i)C(J_i2J_f;M_iMM_f)\equiv\sum_{\text{protons}}\langle\psi_f|r_p^2Y_2^M(\theta_p\phi_p)|\psi_i\rangle. \quad (4)$$

The correlation of the emitted gamma ray with the incident particle is calculated from the formula[6]

$$W(\theta)=A_0+a_2A_2P_2+a_4A_4P_4, \quad (5)$$

where a_2 and a_4 are particle parameters independent of the nuclear transitions, the P_ν are Legendre polynomials,

[6] L. C. Biedenharn and M. E. Rose, Revs. Modern Phys. **25**, 729 (1953).

and the A_ν are the $\gamma-\gamma$ correlation coefficients[6,7] such that the $\gamma-\gamma$ correlation is given by $W(\theta)=\sum_\nu A_\nu P_\nu$.

The particle parameters are

$$a_2=b_2/b_0, \tag{6}$$

$$a_4=b_4/b_0, \tag{7}$$

where

$$\begin{aligned} b_2=\sum_l\Big[&\frac{3(l-2)(l-1)(l)}{(2l-1)^2}I^2(l-2,l)\\ &-\frac{l(l+1)(2l+1)(2l-3)(2l+5)}{(2l-1)^2(2l+3)^2}I^2(l,l)\\ &+\frac{3(l+1)(l+2)(l+3)}{(2l+3)^2}I^2(l+2,l)\\ &-6\cos(\sigma_l-\sigma_{l-2})\frac{l(l-1)(l+1)}{(2l-1)^2}I(l-2,l)I(l,l)\\ &-6\cos(\sigma_l-\sigma_{l+2})\frac{l(l+1)(l+2)}{(2l+3)^2}I(l+2,l)I(l,l)\Big], \end{aligned} \tag{8}$$

and

$$\begin{aligned} b_4=-\frac{1}{16}\sum_l\Big[&\frac{9l(l-1)(l-2)(l-3)}{(2l+1)(2l-1)^2}I^2(l-2,l)\\ &+\frac{36(2l+1)(l+2)(l+1)(l)(l-1)}{(2l+3)^2(2l-1)^2}I^2(l,l)\\ &+\frac{9(l+4)(l+3)(l+2)(l+1)}{(2l+1)(2l+3)^2}I^2(l+2,l)\\ &-60\cos(\sigma_{l-2}-\sigma_l)\frac{(l+1)(l)(l-1)(l-2)}{(2l-1)^2(2l+3)}I(l,l)I(l-2,l)\\ &+210\cos(\sigma_{l-2}-\sigma_{l+2})\frac{(l+2)(l+1)(l)(l-1)}{(2l-1)(2l+1)(2l+3)}\\ &\times I(l-2,l)I(l+2,l)-60\cos(\sigma_l-\sigma_{l+2})\\ &\times\frac{(l+3)(l+2)(l+1)(l)}{(2l-1)(2l+3)^2}I(l,l)I(l+2,l)\Big]. \end{aligned} \tag{9}$$

The particle parameters a_2 and a_4 are dimensionless functions of the two variables $\rho\equiv k_{\text{initial}}/k_{\text{final}}$ and $\eta\equiv Z_1Z_2e^2/\hbar v_{\text{initial}}$. The excitation function b_0 may be expressed in terms of the dimensionless function

$$a_0\equiv(k_{\text{final}})^{-4}b_0. \tag{10}$$

It is this dimensionless function a_0 rather than b_0 which is tabulated below.

[7] S. P. Lloyd, Phys. Rev. **83**, 716 (1951); D. L. Falkoff and G. E. Uhlenbeck, Phys. Rev. **79**, 334 (1950). Additional references may be found in reference 6.

METHOD OF CALCULATION

Since a reasonably accurate determination of the coefficients a_μ requires consideration of a large number of angular momenta, a direct calculation by numerical integration over Coulomb wave functions of the many integrals involved is clearly impractical. For this reason, the analytic procedures development in I greatly facilitate the calculation. Three different methods were discussed in that paper: (a) use of the Appell F_3 function [see I, Eqs. (43), (44), and (101)], (b) use of the Appell F_2 function [see I, Eqs. (43)–(45)], (c) use of recursion relations [see I, Eqs. (65)–(67)].

It did not prove feasible to employ the Appell F_3 function method without modification, because the double series involved does not converge sufficiently rapidly for large values of L or η; the convergence criterion is $(L^2+\eta^2)(\rho-1)\gtrsim 1$. It did, however, prove possible to use the Appell F_2 function method. Since the reduction of the integral $I(l,l)\equiv(0,3;l)$ is not explicitly given in I, the formula is given below:

$$\begin{aligned} &k_2^{-2}(0,3;l)\\ &=\frac{1}{2l}\Big[(1+\rho^2)+\frac{2\rho^2\eta^2(2l+3)}{(l+1)^2(2l+1)}\Big](0,1;l)\\ &\quad-\frac{\rho}{l(l+1)^2}[(l+1)^2+\eta^2]^{\frac{1}{2}}[(l+1)^2+\rho^2\eta^2]^{\frac{1}{2}}(0,1;l+1)\\ &\quad-\frac{\rho\eta}{l(l+1)(2l+1)}\Big\{\Big[\frac{(l+1)^2+\rho^2\eta^2}{(l+1)}\Big]^{\frac{1}{2}}(1,1;l)\\ &\qquad+\rho[(l+1)^2+\eta^2]^{\frac{1}{2}}(-1,1;l+1)\Big\}. \end{aligned} \tag{11}$$

This reduction derives from the recursion relations I, Eqs. (57)–(58) and obviates the necessity for the use of the triple series for $(0,3;l)$, since the function $(0,1;l)$ and $(1,1;l)$ are double series, see I, Eq. (45). The employment of these double series in the F_2 form proved practical for the calculation of the a_μ for energy losses of less than about 20%. A serious disadvantage to this procedure, however, is that it is exceedingly laborious. Nevertheless, this method was useful for calculating a few survey cases[8] and for obtaining check values for other calculational schemes.

The recursion relations could be used in conjunction with the F_2 method to decrease the labor somewhat, by calculating with the F_2 form for given values of l and generating the function at intermediate values of l by recursion. However, care must be taken not to place too much reliance on the recursion procedure since the diverging solutions to these relations unavoidably enter and eventually dominate.

The method which was used in the present work has

[8] Goldstein, McHale, Thaler, and Biedenharn, Phys. Rev. **100**, 435 (1955).

not been given elsewhere and represents a Green's function solution to the inhomogeneous recurrence relations given in I, Eqs. (65) and (67). The formula for $(2,3;l)$ is

$$(2,3;l)=f(l)\left[\frac{(2,3;L)}{f(L)}+\sum_{j=L}^{l-1}\frac{A(j)}{f(j+1)}\right], \quad (12)$$

where

$$f(l)=\rho^l|\Gamma(l+1+i\eta)/\Gamma(l+3+i\rho\eta)|, \quad (13)$$

and

$$A(l)=\left\{\frac{(\rho^2-1)k_2^2}{4(l+1)|l+2+i\rho\eta||l+3+i\rho\eta|}\right\}$$
$$\times\{[2\rho^2\eta^2+\rho^2(l+1)(2l+3)-l-1](0,1;l+1)$$
$$-2\rho|l+1+i\eta||l+1+i\rho\eta|(0,1;l)\}. \quad (14)$$

It is readily seen that $f(l)$ is a solution of the homogeneous recursion relation,

$$f(l+1)-\rho\left|\frac{l+1+i\eta}{l+3+i\rho\eta}\right|f(l)=0, \quad (15)$$

and that Eq. (12) is a solution of the inhomogeneous relation,

$$(2,3;l+1)-\rho\left|\frac{l+1+i\eta}{l+3+i\rho\eta}\right|(2,3;l)=A(l), \quad (16)$$

where $A(l)$ is defined by Eq. (14).

Similarly, the formula for $(0,3;l)$ is

$$(0,3;l)=F_l\sum_{j=L+1}^{l-1}\frac{d_jG_j}{a_j(F_{j+1}G_j-F_jG_{j+1})}$$
$$-G_l\sum_{j=L+1}^{l-1}\frac{d_jF_j}{a_j(F_{j+1}G_j-F_jG_{j+1})}$$
$$+F_l\left[\frac{G_L(0,3;L+1)-G_{L+1}(0,3;L)}{(F_{L+1}G_L-F_LG_{L+1})}\right]$$
$$-G_l\left[\frac{F_L(0,3;L+1)-F_{L+1}(0,3;L)}{(F_{L+1}G_L-F_LG_{L+1})}\right], \quad (17)$$

where

$$F_l=\rho^{-l}\left|\frac{\Gamma(l+1+i\rho\eta)}{\Gamma(l+1+i\eta)}\right|\frac{1}{l(l+1)(2l+1)}, \quad (18)$$

$$G_l=\rho^{l}\left|\frac{\Gamma(l+1+i\eta)}{\Gamma(l+1+i\rho\eta)}\right|\frac{1}{l(l+1)(2l+1)}, \quad (19)$$

$$d_l=-\tfrac{3}{4}l(l+1)(2l+1)k_2^4(1-\rho^2)^2(0,1;l), \quad (20)$$

and

$$a_l=l(l+2)(2l+3)k_2^2\rho|l+1+i\eta||l+1+i\rho\eta|. \quad (21)$$

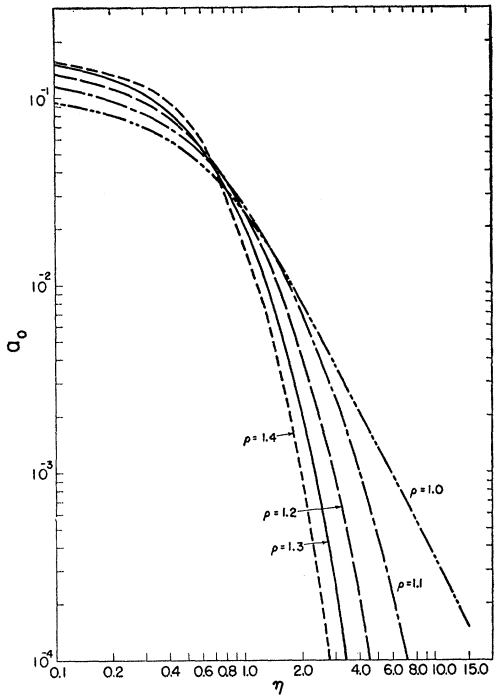

FIG. 1. The excitation coefficient a_0 *vs* η on a log-log plot for several values of constant ρ.

The use of this method merely requires the generation of a few initial values of the functions $(2,3;l)$ and $(0,3;l)$ and the calculation of the function $(0,1;l)$. Values for $(2,3;l)$ for low l were easily obtained using the F_3 method. The function $(0,1;l)$ is a reducible Appell function and can be represented as an ordinary hypergeometric function.[9]

It is clear that this method has several important advantages. First, the amount of labor required in the computation is reduced more than a hundred fold. This circumstance arises mainly from the fact that the Appell functions are exceedingly difficult to calculate in contrast to the ordinary hypergeometric function. Second, this method makes it feasible to calculate over a much greater range of the arguments ρ, η. With this method, one may calculate for energy losses of up to 75% for a very wide range of values of η. Moreover, the attendant numerical error is considerably reduced in this procedure. Unlike the recursion relations from which these formulas derive, the error does not accumulate with increasing l. Rather, the error in the function $(-2,3;l)$ diminishes as l is increased and even errors in the starting values become increasingly less important, since the sum dominates the initial values. On the other hand the error in $(2,3;l)$ increases with l since the sum tends eventually to cancel the initial value. Fortunately, this is of little consequence, since the contribution to the a_μ of the $(-2,3;l)$ dominates that of the $(2,3;l)$ before

[9] A. J. F. Sommerfeld, *Atombau und Spektrallinien* (Ungar, New York, 1950), Vol. 2.

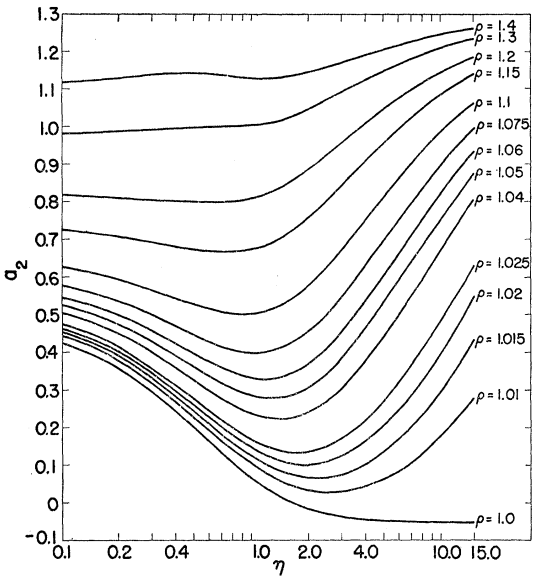

FIG. 2. The particle parameter a_2 *vs* η on a semilog plot for constant values of ρ.

the error in the latter becomes significant. Similarly, the $(0,3;l)$ contains a part in which the error decreases with l and a part in which the error increases with l, but again the contribution of the former dominates that of the latter before the error in the latter becomes significant.

Initial values for the recursion were generated by means of the F_3 method rather than by means of the F_2 method because the F_3 representation has the same form for the different integrals involved [see I, Eqs. (43), (44), and (101)] whereas in the F_2 method the $(0,3;l)$ must be treated differently from the $(2,3;l)$ [see Eq. (11) and I, Eqs. (43)–(45)].

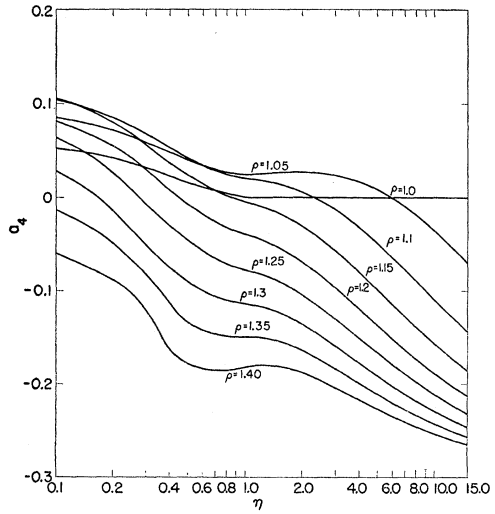

FIG. 3. The particle parameter a_4 *vs* η on a semilog plot for constant values of ρ.

RESULTS

Some of the numerical results are presented in the accompanying tables. The coefficients a_0, a_2, and a_4 are given to four figures in Tables I, II, and III, respectively; the arguments ρ, η in these tables have the ranges $1.01 \leqslant \rho \leqslant 1.4$ and $0.1 \leqslant \eta \leqslant 15$. It is believed that these numbers are accurate to within one or two units in the last place. The region of greatest inaccuracy is for ρ, η large. In the region of interest for analysis of the present experiments,[2] *viz.*, $2 \leqslant \eta \leqslant 8$, $1.02 < \rho < 1.2$, the results are believed to be accurate to four figures as presented. Examination of the error introduced term by term in the present calculation provided confirmation of this accuracy. Typical values were also checked independently by means of the F_2 and F_3 methods.

The tables are supplemented by the accompanying graphs which display some of the qualitative features of

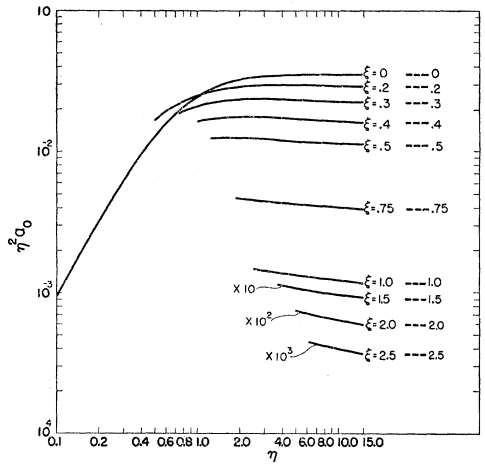

FIG. 4. The quantity $\eta^2 a_0$ *vs* η on a log-log plot for constant values of the classical variable ξ. The curves are given for $\rho \leqslant 1.4$, $\eta \leqslant 15$. The dashed lines on the right represent the asymptotic values[10] of these curves in the limit $\eta \to \infty$, and are labeled with the value of ξ. The lowest three curves are scaled by different factors of ten, as indicated in the figure. (*Note.*—The ordinate is incorrectly labeled and should run from 10^{-4} to 10^{-1}.)

these results. In Fig. 1 the dimensionless excitation coefficient a_0 is shown as a function of η on a log-log plot for constant values of ρ. In Figs. 2 and 3 the particle parameters a_2, a_4 are plotted against $\log\eta$ for constant values of ρ.

The very rapid variation of a_0 as a function of η, as exhibited in Fig. 1, shows that care must be taken in interpolating in Table I. Clearly, interpolation in η is best accomplished by interpolating $\log a_0$. The particle parameters a_2, a_4 (see Figs. 2, 3), on the other hand, do not vary nearly so rapidly as functions of η and are more easily interpolated. For values of $\eta > 2$, the functions a_2 and a_4 are best interpolated with respect to η, whereas for smaller values of the argument, the functions are best interpolated with respect to $\log\eta$.

The function a_0 for constant values of η is likewise a rapidly varying function of ρ for large values of ρ, so

that interpolation in ρ for large values of ρ is best accomplished by interpolating $\log a_0$; for small values of ρ, however, a_0 is slowly varying and is easily interpolated directly. The particle parameters a_2 and a_4, for constant values of η are, on the other hand, slowly varying functions of ρ, so that interpolation in ρ presents no difficulties. Because of space limitations, plots of the a_μ *vs* ρ for constant η are not shown.

It is seen in Figs. 2 and 3 that the particle parameters a_2 and a_4 are especially sensitive to small changes in ρ near the zero-energy-loss limit ($\rho=1$) for large η. The curves for a_4 cross in Fig. 3 since a_4 has a maximum as a function of ρ for constant η.

As η approaches infinity and ρ approaches unity, the function $\eta^2 a_0$ and the particle parameters a_2, a_4 become functions of the single classical variable $\xi \equiv \eta(\rho-1)$. In

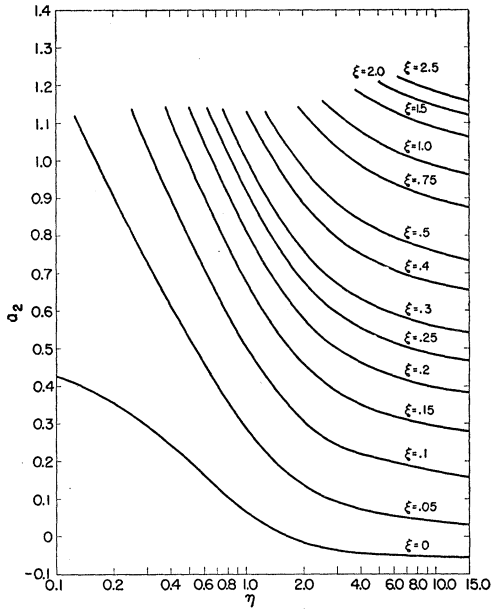

FIG. 5. The particle parameter a_2 *vs* η on a semilog plot for constant values of the classical variable ξ. The curves are given for $\rho \leqslant 1.4$, $\eta \leqslant 15$.

Figs. 4–6 are shown curves of these functions (i.e., $\eta^2 a_0$, a_2, a_4) plotted against $\log\eta$ for constant values of ξ. These plots for constant ξ indicate the manner in which these functions approach their classical limiting values as η increases. The smaller the value of ξ, the more rapidly is the limit approached as a function of η since the classical limit implies $\rho \rightarrow 1$, as well as $\eta \rightarrow \infty$. The classical limits for $\eta^2 a_0$ obtained by Alder and Winther[10] are shown in Fig. 4. Classical limits for a_2 and a_4 are not available at present, although extrapolation of the curves in Figs. 5 and 6 should give good estimates of these limiting values. As expected, Figs. 4–6 show large deviations from the classical results for small values of η and large values of ρ. In regions where deviations from

[10] K. Alder and A. Winther, CERN/TKA-AW-1, October, 1954 (unpublished).

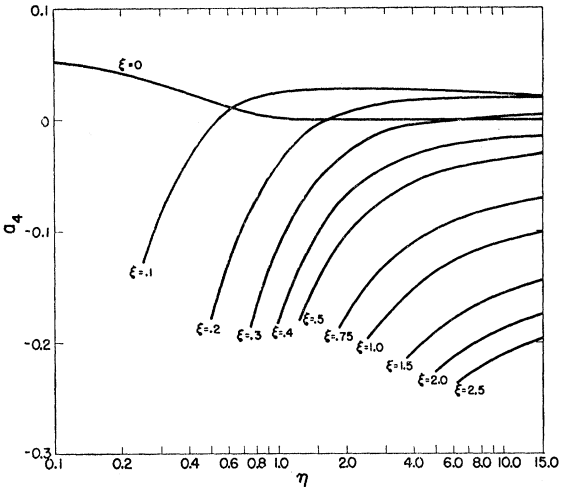

FIG. 6. The particle parameter a_4 *vs* η on a semilog plot for constant values of the classical variable ξ. The curves are given for $\rho \leqslant 1.4$, $\eta \leqslant 15$.

the classical limits are not extreme, this type of plot is useful for interpolation.

The apparently anomalous position of the $\xi=0$ curve in Fig. 6 follows from the fact that a_4 has a maximum as a function of ξ for fixed η. At $\eta=15$ this maximum lies between $\xi=0.1$ and $\xi=0.2$; at $\eta=1$ the maximum is between $\xi=0$ and $\xi=0.1$.

DISCUSSION

The effect of increasing η is to enhance the contributions to the functions b_μ of the higher angular momenta, shifting the peak contribution to a higher value of l. On the other hand, the effect of increasing ρ is to diminish the importance of the higher angular momenta. Thus, keeping $\eta(\rho-1)$ constant tends to keep the summed contributions of the various angular momenta roughly

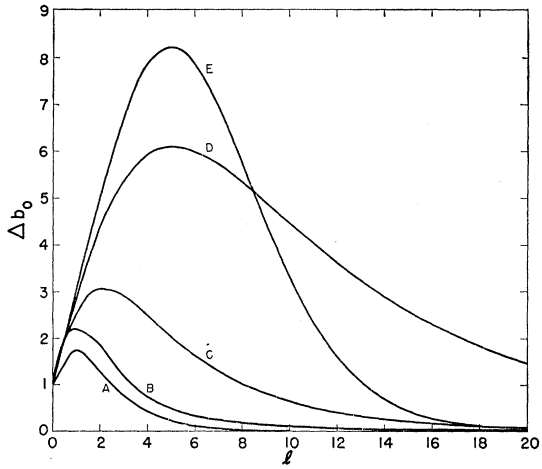

FIG. 7. Increment of the excitation function b_0 *vs* angular momentum l. These curves are normalized to unity at $l=0$. For curve A, $\rho=1.4$, $\eta=2$; for curve B, $\rho=1.05$, $\eta=2$; for curve C, $\rho=1.1$, $\eta=4$; for curve D, $\rho=1.05$, $\eta=8$; for curve E, $\rho=1.4$, $\eta=8$.

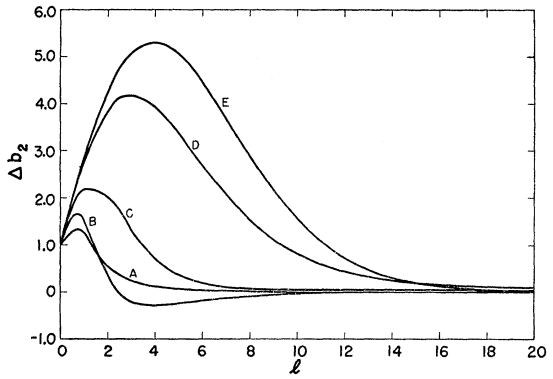

FIG. 8. Increment of the function b_2 *vs* angular momentum l. These curves are normalized to unity at $l=0$. For curve A, $\rho=1.4$, $\eta=2$; for curve B, $\rho=1.05$, $\eta=2$; for curve C, $\rho=1.1$, $\eta=4$; for curve D, $\rho=1.05$, $\eta=8$; for curve E, $\rho=1.4$, $\eta=8$.

constant. This provides some indication of the utility of the classical variable $\xi=\eta(\rho-1)$.

The fact that large η implies high angular momenta is due to the simultaneous effects of the barrier and degeneracy in angular momentum. The effect of the increased barrier due to larger η is to diminish the importance of the lowest angular momenta such that all angular momenta below the barrier contribute roughly to the same order. Thus, increasing η will increase the number of l's which enter significantly. In addition, degeneracy favors the contributions of the higher angular momenta by a factor of the order of l.

Large ρ, i.e., large energy loss, implies large decelerations and hence small impact parameters. Thus, as ρ increases for constant η, the contributions of the higher angular momenta are increasingly suppressed. These qualitative conclusions are not altered by the action of the barrier on the scattered particle, despite the fact that this effect is in the opposite direction.

The qualitative considerations discussed above are shown in Figs. 7–9. In these figures the increment to b_μ is plotted as a function of l. Five cases have been chosen as illustrations: (I) $\eta=2$, with $\rho=1.4$ (curves A) and $\rho=1.05$ (curves B); (II) $\eta=8$, with $\rho=1.4$ (curves E) and $\rho=1.05$ (curves D); (III) $\rho=1.05$, with $\eta=2$ (curves B) and $\eta=8$ (curves D); (IV) $\rho=1.4$, with $\eta=2$ (curves A) and $\eta=8$ (curves E); (V) $\xi=0.4$, with $\rho=1.1$, $\eta=4$ (curves C) and $\rho=1.05$, $\eta=8$ (curves D). These curves have been normalized such that the contribution for $l=0$ is unity.

Case I shows the effect of extreme variation in ρ for small $\eta=2$. It is seen that curves A tail off more rapidly than curves B, in accordance with the arguments above. Similarly, Case II illustrates this same effect for large $\eta=8$.

For $\rho\sim1$, the maximum occurs at $l\sim\eta$. Moreover, it is seen that the positions of the maxima depend primarily on η and in general are not particularly sensitive to the value of ρ. Case III shows the effect of variation in η for small ρ. It is again seen that the position of the peak occurs further out for large η than for small. Similarly, Case IV illustrates this same effect for large $\rho=1.4$.

Case V shows the effect of changes in ρ, η for a fixed value of the classical variable $\xi=\eta(\rho-1)=0.4$. It is seen that curves C ($\rho=1.1$, $\eta=4$) peak at lower values of l and fall off more rapidly than curves D ($\rho=1.05$, $\eta=8$), as expected from the discussion above. Despite the

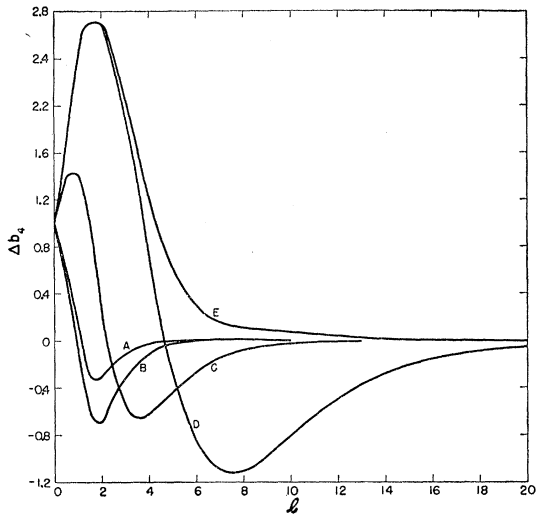

FIG. 9. Increment of the function b_4 *vs* angular momentum l. These curves are normalized to unity at $l=0$. For curve A, $\rho=1.4$, $\eta=2$; for curve B, $\rho=1.05$, $\eta=2$; for curve C, $\rho=1.1$, $\eta=4$; for curve D, $\rho=1.05$, $\eta=8$; for curve E, $\rho=1.4$, $\eta=8$.

dissimilar behavior of these two examples as functions of l, the final values of the quantities $\eta^2 a_0$, a_2, and a_4 are roughly equal, *viz.*, 0.017, 0.75, and -0.03 for C as compared with 0.017, 0.69, and -0.02 for D.

The oscillations about zero of the curves in Fig. 9 indicate why the particle parameter a_4 is generally small.

ACKNOWLEDGMENTS

The authors wish to thank Mr. Ivan Cherry and Mrs. Bertha Fagan for assistance in coding this problem for the Los Alamos IBM 701 computers, and Miss Barbara Blanchard for help in preparation of the manuscript.